AGU PUBLICATIONS

JGR

Journal of Geophysical Research: Planets

RESEARCH ARTICLE

10.1002/2013JE004494

Key Points:
- A heterogeneous and wet mantle could have increased core dynamo by up to 2.0 Gyr
- Enriched water could have influenced core dynamo timing by up to 1.0 Gyr
- Plausibility of convective lunar dynamo beyond period indicated by lunar samples

Correspondence to:
A. J. Evans,
ajevans@alum.mit.edu

Citation:
Evans, A. J., M. T. Zuber, B. P. Weiss, and S. M. Tikoo (2014), A wet, heterogeneous lunar interior: Lower mantle and core dynamo evolution, *J. Geophys. Res. Planets*, *119*, 1061–1077, doi:10.1002/2013JE004494.

Received 27 JUL 2013
Accepted 22 FEB 2014
Accepted article online 13 MAR 2014
Published online 14 MAY 2014

A wet, heterogeneous lunar interior: Lower mantle and core dynamo evolution

A. J. Evans[1,2], M. T. Zuber[1], B. P. Weiss[1], and S. M. Tikoo[1]

[1]Department of Earth, Atmospheric and Planetary Sciences, Massachusetts Institute of Technology, Cambridge, Massachusetts, USA, [2]Lamont-Doherty Earth Observatory, Columbia University, Palisades, New York, USA

Abstract While recent analyses of lunar samples indicate the Moon had a core dynamo from at least 4.2–3.56 Ga, mantle convection models of the Moon yield inadequate heat flux at the core-mantle boundary to sustain thermal core convection for such a long time. Past investigations of lunar dynamos have focused on a generally homogeneous, relatively dry Moon, while an initial compositionally stratified mantle is the expected consequence of a postaccretionary lunar magma ocean. Furthermore, recent re-examination of Apollo samples and geophysical data suggests that the Moon contains at least some regions with high water content. Using a finite element model, we investigate the possible consequences of a heterogeneously wet, compositionally stratified interior for the evolution of the Moon. We find that a postoverturn model of mantle cumulates could result in a core heat flux sufficiently high to sustain a dynamo through 2.5 Ga and a maximum surface, dipolar magnetic field strength of less than 1 μT for a 350-km core and near ~2 μT for a 450-km core. We find that if water was transported or retained preferentially in the deep interior, it would have played a significant role in transporting heat out of the deep interior and reducing the lower mantle temperature. Thus, water, if enriched in the lower mantle, could have influenced core dynamo timing by over 1.0 Gyr and enhanced the vigor of a lunar core dynamo. Our results demonstrate the plausibility of a convective lunar core dynamo even beyond the period currently indicated by the Apollo samples.

1. Introduction

The Moon is posited to have formed from the coalescence of postimpact debris of a protoplanet with the young Earth [*Cameron and Ward*, 1976; *Cameron*, 1986]. Following the giant impact of the Earth with a planetary embryo, material scattered beyond the Roche limit into a protolunar disk and subsequently aggregated to form the Moon [*Cameron*, 1986; *Cameron and Ward*, 1976; *Canup and Asphaug*, 2001; *Canup*, 2004]. The anorthositic composition of the lunar highlands and KREEP (potassium, rare earth elements, and phosphorus) terrane of the lunar nearside [*Jolliff et al.*, 1999] support the past existence of a large-scale lunar magma ocean leading to fractional crystallization and compositional stratification of the Moon [*Wood et al.*, 1970; *Wood*, 1972; *Warren*, 1985]. Although a 40-to 50-km anorthositic lunar crust is consistent with a magma ocean depth of up to 1000 km [*Elkins-Tanton et al.*, 2011], a lower magma ocean depth limit may be likely given recent observational data from the dual Gravity Recovery and Interior Laboratory (GRAIL) spacecraft [*Zuber et al.*, 2013] that indicates an average crustal thickness between 34 and 43 km [*Wieczorek et al.*, 2013].

During the final stages of fractional crystallization from a lunar magma ocean, the last dregs of the melt would be enriched in water and incompatible elements, subsequently crystallizing beneath the anorthositic crustal lid [*Hess and Parmentier*, 2001; *Wieczorek and Phillips*, 2000]. Furthermore, fractional crystallization would result in a chemically layered mantle, which may be supported by some seismic observations [*Wieczorek and Phillips*, 1998]. Until recently, the Moon had been thought to have a relatively low volatile content due to a combination of its low-gravity and hot impact origin [*Lucey et al.*, 2006; *Pahlevan and Stevenson*, 2011]. Accordingly, past studies of the Moon's formation and its chemical and thermal evolution have focused on a bulk Moon with minimal volatile content and the absence of water [*Shearer*, 2006]. However, recent geochemical analyses of very low Ti glasses and lunar melt inclusions present compelling evidence that water concentrations of at least 260 ppm and up to 6000 ppm were present in some regions of the lunar interior prior to 3 Ga [*Saal et al.*, 2008; *Hauri et al.*, 2011]. Furthermore, analysis of the electrical conductivity of the Moon suggests a reduced viscosity layer above the core-mantle boundary consistent with an enriched wet region of approximately 100–200 km [*Karato*, 2013; *Khan et al.*, 2013]. If water was

Table 1. Parameter Values for Thermochemical Evolution Model[a]

Parameter	Value
Activation energy, E	5.0×10^5 J mol^{-1}
Activation volume, V	1.5×10^{-6} m^3 mol^{-1}
Crustal thickness	50 km
Core density, ρ_{core}	7400 kg m^{-3}
Core radius, R_c	350 km
Core conductivity, k_{core}	25 W/m K
Core specific heat capacity, $c_{p,core}$	800 J/K
Core temperature, T_c	1800 K
Core thermal expansivity, α_c	5.85×10^{-5} K^{-1}
Specific heat capacity, $c_{p,mantle}$	1200 J/K
Mean planetary radius, R_p	1737 km
Rayleigh number, Ra	10^6–10^8
Thermal diffusivity, κ	10^{-6} m^2 s^{-1}
Thermal expansivity, α	3×10^{-5} K^{-1}
Shear modulus, μ	5×10^{10} N m^{-2}
Surface gravity, g	1.63 m s^{-2}
Viscosity, maximum variation	10^9
Viscosity, minimum variation	10^{-2}
Viscosity reference, η_0	10^{19}–10^{21} Pa s
Surface temperature, T_s	250 K

[a]Values for core are based on *Stegman et al.* [2003] and *Dwyer et al.* [2011]; mantle and surface values are based on *Elkins-Tanton et al.* [2003]; and rheological values are from *Zhong et al.* [2000b].

a constituent of the bulk Moon, fractional crystallization of all but the deep mantle would have resulted in a sequestered source of interior water. Ultimately, in this scenario, a postmagma ocean Moon would contain separate subcrustal and deep mantle reservoirs, which may be consistent with both localized water-rich reservoirs (≥260 ppm) [*Saal et al.*, 2008] and a bulk magma ocean containing under 100 ppm water [*Elkins-Tanton and Grove*, 2011].

It remains unclear if lunar water is terrestrial in origin as deuterium to hydrogen (D/H) ratios of measured lunar water in apatite are consistent with a cometary origin [*Greenwood et al.*, 2011]. However, the observed hydrogen fractionation could have alternatively resulted from water-rich glasses that erupted from a source region with terrestrial D/H values, provided the glasses had undergone kinetic fractionation during post-eruptive degassing [*Saal et al.*, 2012]. This may be consistent with *Pahlevan and Stevenson* [2011], which find, absent removal mechanisms that may be responsible for later depletion of volatiles, a postformation enhancement of terrestrial-imparted volatiles may be an expected consequence of lunar formation. Regardless of whether the lunar water is indigenous, exogenous, or a combination thereof, water in the deep lunar interior must have been retained from accretion or accreted prior to and conceivably during lunar magma ocean solidification. Under the lunar magma ocean model, water would be progressively enriched with incompatible elements during solidification, and a fraction may have been retained by the lunar mantle [*Warren and Wasson*, 1979; *Elkins-Tanton and Grove*, 2011]. Although it is unclear whether measured water concentrations are representative of the entire lunar mantle or a water-enriched reservoir [*Hauri et al.*, 2011], the existence and subsequent enrichment of water in the lunar interior could well have had a significant effect on early lunar thermochemical evolution [*Shearer*, 2006; *Hirth and Kohlstedt*, 1995; *Karato*, 2010]. In particular, water may have aided the cooling of the early Moon [*Neumann et al.*, 1996; *Hood and Zuber*, 2000] in addition to influencing the expression of surface features such as impact basins.

Unlike the Earth [*Bercovici and Karato*, 2003], deep reservoirs of water within the Moon could possibly exist near the core-mantle boundary and, if so, could decrease lower mantle viscosity, possibly facilitating a prolonged and conceivably vigorous lunar dynamo. While the size and composition of the lunar core are still a matter of active investigation, analyses with recent lunar data indicate the Moon may have a maximum outer core radius of 380 km surrounding a solid inner core with a radius up to 200 km (J. G. Williams et al., Lunar interior properties from the GRAIL mission, submitted to *Journal of Geophysical Research-Planets*, 2013). Recent analyses of lunar samples indicate that the Moon had a dynamo-driven magnetic field from at least 4.2–3.56 Ga, consistent with the presence of a convecting liquid iron-rich core [*Garrick-Bethell et al.*, 2009; *Cournède et al.*, 2012; *Shea et al.*, 2012; *Suavet et al.*, 2013]. Given bounds on the lunar core size [*Weber et al.*, 2011; *Runcorn*, 1996; J. G. Williams et al., unpublished data, 2013], it may be implausible for lunar mantle convection from secular cooling to generate such a long-lasting dynamo via core convection [*Suavet et al.*, 2013; *Laneuville et al.*, 2013] without mediation by a thermal blanket [*Stegman et al.*, 2003; *Zhang et al.*, 2013], impact-induced rotation changes [*Le Bars et al.*, 2011], or, possibly, a water-rich layer near the core-mantle boundary.

Although the cooling history of the Moon is still ambiguous, there is some evidence, including recovered lunar alkalic igneous rocks, indicative of a late, rapid cooling scenario for the shallow Moon, which may have been preceded by, or overlapped with, a slow cooling phase of the deep Moon [*Jolliff et al.*, 1999; *McCallum and Schwartz*, 2001; *Longhi and Ashwal*, 1985]; such a scenario would be consistent with a convective core dynamo. In this study, we address the influence of water on lunar evolution by incorporating an attenuating

Table 2. Parameter Values for the Radioactive Content[a]

Concentration	Crust	KREEP	Mantle
Thorium	800 ppb	12.4 ppm	25 ppb
Uranium	130 ppb	3.4 ppm	4.0 ppb
Potassium	320 ppm	5100 ppm	10 ppm

[a]Values are based on potassium, thorium, and uranium concentrations from *Taylor et al.* [2013, 2006] and measurements from lunar samples [*Warren and Wasson*, 1979; *Wieczorek and Phillips*, 2000; *Korotev*, 2000]. For numerical reasons, we model a 2.5-km thick KREEP layer to have a thickness of 19 km with the concentrations reduced accordingly.

strain rate as a proxy for decreased viscosity [*Shearer*, 2006; *Hirth and Kohlstedt*, 1995; *Kohlstedt*, 2006] for potential wet regions in the lunar interior. From experimental studies of the Earth's upper mantle (300 MPa), the presence of a small amount of water (~40 wt ppm) can result in a viscosity reduction by a factor in excess of 100 [*Hirth and Kohlstedt*, 1995; *Kohlstedt*, 2006]. We examine the influence of compositional stratification and water via protonic weakening [*Kohlstedt*, 2006] —proton diffusion into nominally anhydrous minerals—on the deep interior. We utilize a finite element thermochemical evolution model and investigate changes in temperature, modes of heat transport, core-mantle boundary heat flux, and surface magnetic field intensity. We then use the core-mantle boundary heat flux to provide constraints on the duration of core dynamo activity.

2. Methodology

2.1. Thermochemical Evolution

We employ a modified version of the spherical axisymmetric, finite element thermochemical evolution (convective and conductive heat transport) code, Citcom2D [*Moresi and Solomatov*, 1995; *Zhong et al.*, 2000a; *Roberts and Zhong*, 2004] on a 256 × 96 gridded element mesh that models two-dimensional, incompressible mantle evolution with the Boussinesq approximation through the nondimensionalized governing equations of the conservation of mass, momentum, and energy,

$$u_{i,i} = 0 \tag{1}$$

$$-P_{,j} + \left[\eta(r,T)\left(u_{i,j} + u_{j,i}\right)\right]_{,j} + Ra\,(T - \beta C)\,\delta_{i,r} = 0 \tag{2}$$

$$\dot{T} + u_i T_{,i} = \kappa T_{,ii} + H(t) \tag{3}$$

with

$$\dot{C} + u_i C_{,i} = 0 \tag{4}$$

where $\vec{u}$ is the velocity vector, P is the dynamic pressure, Ra is the Rayleigh number referenced to the lunar radius, β is the buoyancy number calculated from the difference in density and reference density, r is the radius, T is the temperature, and C is the local density normalized to the reference density, 3000 kg m^{-3}, and maximum density, 3500 kg m^{-3} on a scale of 0 to 1, respectively. In the above equations, we employ Einstein notation to indicate summation over repeated indices, with a subscript comma denoting the derivative with respect to the following spatial index. Values used for our thermochemical evolution model are listed in Table 1. We modify this formalism to allow for a time-dependent heat source, $H(t)$, to account for radioactive decay (Table 2) and we incorporate a depth- and temperature-dependent viscosity,

$$\eta(r,T) = A\eta_o \exp\left[\frac{E' + V'(1-r)}{T + T'_s} - \frac{E' + V'(1 - r_{\text{core}})}{1 + T'_s}\right] \tag{5}$$

$$E' = \frac{E}{R\Delta T}, V' = \frac{\rho g V R_p}{R\Delta T}, T'_s = \frac{T_s}{\Delta T}$$

Table 3. Parameter Values for Magnetic Field Intensity

Parameter	Value
Ratio of dipolar to total magnetic field strength, f_{dip}	1/7
Ratio of ohmic to total dissipation, f_{ohm}	1
Constant of proportionality, c	0.63
Magnetic permeability of free space, μ_o	1.26×10^{-6} H m^{-1}

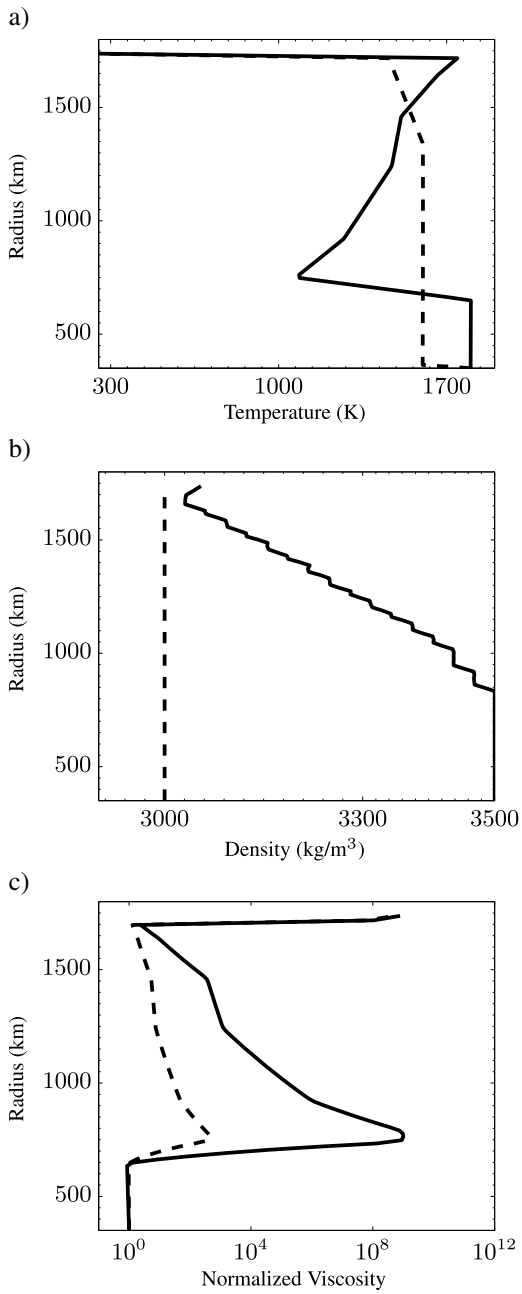

Figure 1. Initial average (a) temperature, (b) density, and (c) viscosity radial profiles used in our evolution models with $\Delta T_{\mathrm{cmb}} = 200$ K. The temperature profile (average temperature (K)) of the deep LMO scenario (solid line) as determined by *Elkins-Tanton et al.* [2011] compared to the shallow LMO (dashed line) is shown in Figure 1a. The density (kg/m^3) profile of the deep LMO scenario (solid line) and the shallow LMO (dashed line) are shown in Figure 1b plotted with radius (km). The initial, radially averaged viscosity profile normalized to the reference viscosity in equation (5) (solid line) and the temperature-damped viscosity in equation (7) (dashed line) is shown in Figure 1c.

where E', V', and T_s' are the nondimensionalized activation energy, E, activation volume, V, and surface temperature, T_s, respectively [*Roberts and Zhong*, 2006; *Korenaga*, 2009], and η_o is the reference viscosity. The parameter ΔT represents the temperature difference across the mantle, g is the lunar surface gravity, r_{core} is the assumed core radius, and A is a dimensionless pre-exponential factor, herein used to incorporate a local viscosity reduction. We apply this viscosity equation in sections 3.1 and 3.2.

To model the cooling of the core-mantle boundary (CMB), we adjust the model to allow for a time-varying CMB thermal boundary condition based on

$$\dot{T}_{\mathrm{cmb}} = \frac{-k_m T_{,r} S}{\left(\rho C_p V\right)_{\mathrm{core}}} \tag{6}$$

where $T_{,r}$ is the average radial temperature gradient above the CMB, S is the surface area, V is the volume of the core, k_m is mantle conductivity, ρ is the core density, and C_p is the core specific heat capacity. Additionally, we use a particle tracer method [*Zhong et al.*, 2007] to allow for radially varying density structures. In addition to bottom heating, we include volumetric heating of the mantle, crust, and KREEP layer with the radioactive element concentrations listed in Table 2.

Prior lunar mantle convection models [*Stegman et al.*, 2003; *Zhong et al.*, 2000b] have applied a variant of the viscosity equation

$$\eta(P,T) = A\eta_o \exp\left[a\frac{E+PV}{RT}\right] \tag{7}$$

with a partially nondimensionalized viscosity equation [*Yang and Baumgardner*, 2000] that damps the temperature dependence of viscosity, where P is the local pressure based on a CMB gravity of 0.9 m/s^2.

The key difference in heat flux predicted by the two viscosity equations is a result of the damping of the temperature dependence by a scale factor, a. This constant a is partially offset by the omission of a second exponential term that references viscosity to the CMB as in equation (5). In section 3.2.2, we use this variant of the viscosity equation as a proxy for a set of scenarios in which the preoverturn temperature of the magma ocean cumulates is not completely retained and to illustrate the differences in applying a rheological equation that does not fully account for the temperature dependence of viscosity. We normalize the viscosity at the CMB to our reference viscosity.

2.2. Water, Pressure, and Rheology

While there has been a recent suggestion [e.g., *Fei et al.*, 2013] that silicon self-diffusion may be a prohibitive factor for water-induced viscosity reduction,

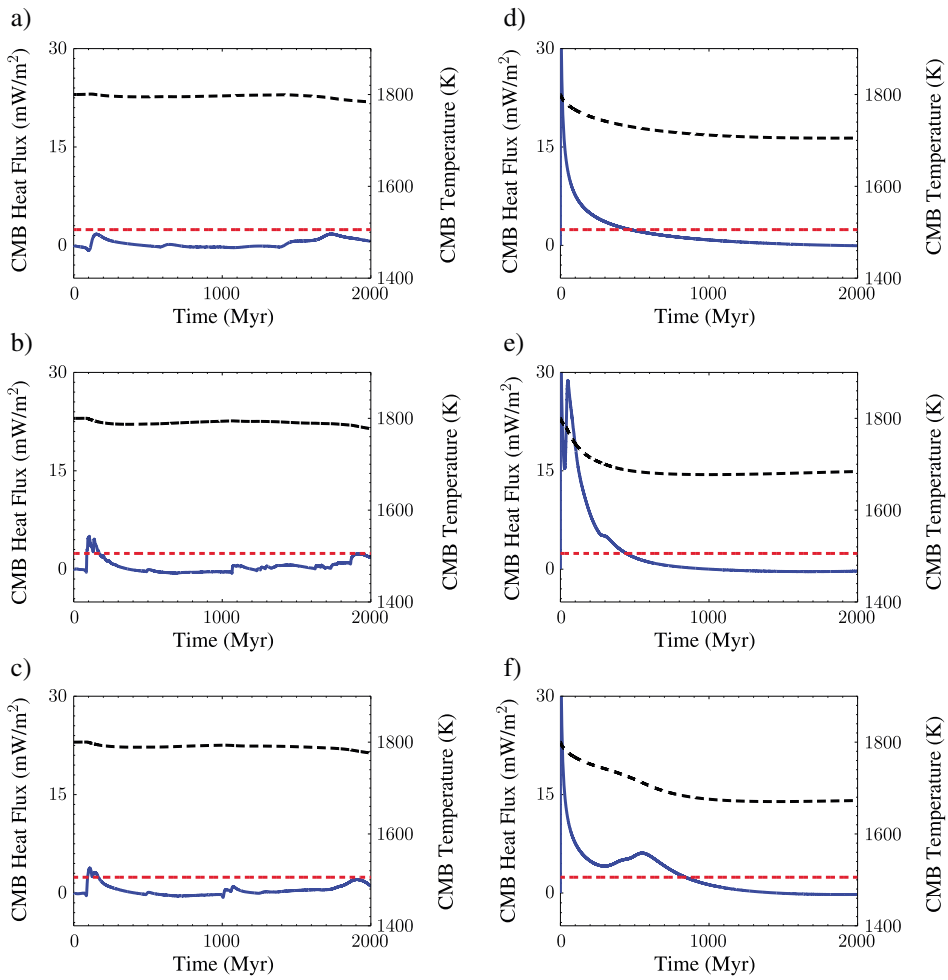

Figure 2. CMB heat fluxes for shallow lunar magma ocean model and reference viscosity of 10^{20} Pa s. The CMB heat flux (blue solid line) is shown on the left axis with the minimum heat flux needed to sustain a core dynamo (red dash-dotted line) and the core temperature (black dashed line) on the right axis. (a–c) Models with $\Delta T_{\mathrm{cmb}} = 0$ K. (d–f) Models with $\Delta T_{\mathrm{cmb}} = 200$ K. Figure 2a shows Case S01: No water enrichment; Figure 2b shows Case S02: 200-km water-enriched layer with 40 ppm water; Figure 2c shows Case S05: 500-km water-enriched layer with 20 ppm water; Figure 2d shows Case S31: No water enrichment; Figure 2e shows Case S32: 200-km water-enriched layer with 40 ppm water; and Figure 2f shows Case S35: 500-km water-enriched layer with 20 ppm water.

experimental studies of olivine aggregates and single crystals indicate that viscosity is reduced in the presence of water (protons) [*Hirth and Kohlstedt*, 1996; *Mackwell et al.*, 1985; *Girard et al.*, 2013]. *Hirth and Kohlstedt* [1996] found that viscosity is reduced by up to a factor of 140 for saturated olivine, corresponding to 40 ± 20 ppm H, at confining pressures of 300 MPa. Their re-examination of higher-pressure data from *Borch and Green* [1989] further suggests that the viscosity reduction factor is directly proportional to the concentration of water in the olivine crystal matrix. Consequently, with the pressure-dependent increase of water solubility in olivine, we may expect a maximum viscosity reduction factor in excess of 140 for a deep lunar mantle (≥300 MPa) preferentially enriched in water and below a factor of 140 at the near surface given the lower pressure.

2.3. Core Heat Flux and Magnetic Field Intensity

We consider a core dynamo driven by thermal core convection and neglect core crystallization. In this case, a necessary but not sufficient condition for an internally generated magnetic field on the Moon is a heat flux at the CMB above the critical threshold value, q_{ad}, of that carried conductively along the core adiabat, where

$$q_{\mathrm{ad}} = \frac{4\pi G \alpha_c \rho_{\mathrm{core}} T_c k_c R_c}{3 c_{p,\mathrm{core}}}. \tag{8}$$

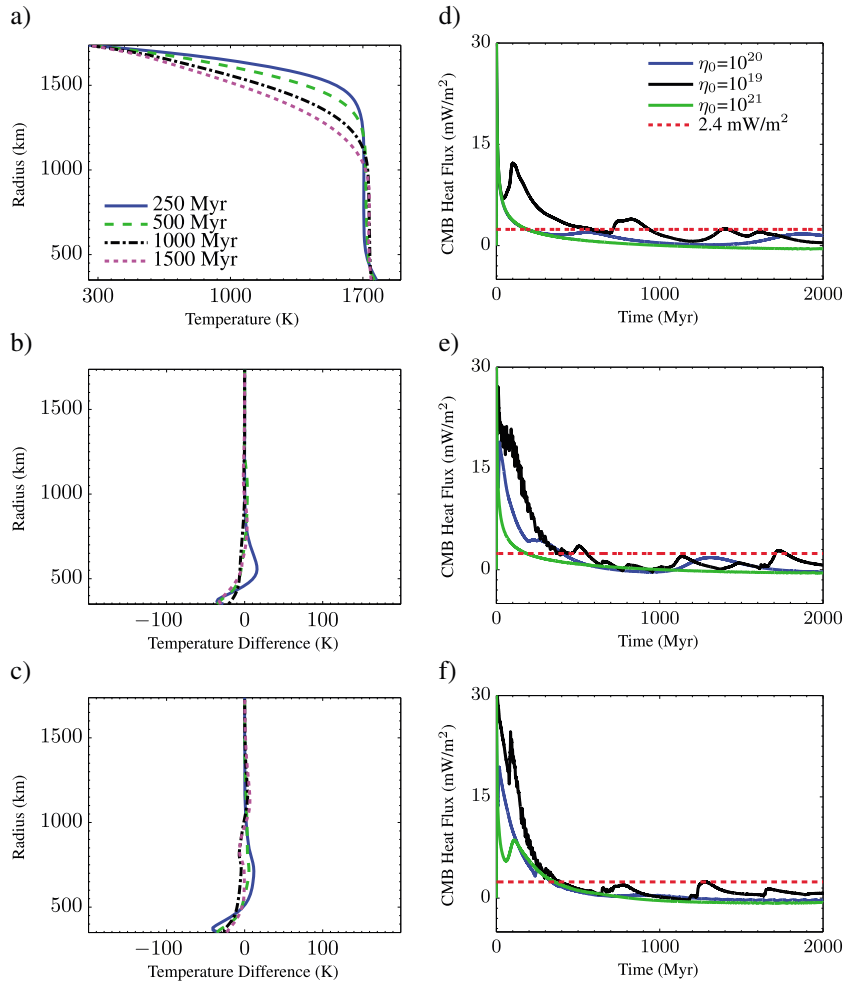

Figure 3. Temperatures and CMB heat fluxes for shallow lunar magma ocean model with $\Delta T_{cmb} = 100$ K. (a and d) Case S25: No water enrichment. (b and e) Case S26: 200 km water-enriched layer with 40 ± 20 ppm water. (c and f) Case S27: 500 km water-enriched layer with 40 ± 20 ppm water. Figures 3b and 3c show the mantle temperature differences relative to the nonwater-enriched scenario for water-enriched models. In Figures 3d–3f, CMB heat flux is shown in models with different reference viscosities $\eta_0 = 10^{19}$ (black line), $\eta_0 = 10^{20}$ (blue line), and $\eta_0 = 10^{21}$ (green line) as a function of model start time with the minimum heat flux needed to sustain a core dynamo (red dash-dotted line).

We define the relevant variables in Table 1. Using the energy flux to magnetic field strength scaling of *Christensen et al.* [2009] and assuming constant material properties in the core (see Table 3), we employ the following relation as an approximation for the surface magnetic field intensity that can be produced from our core heat flux,

$$B_d = f_{\mathrm{dip}} \left(\frac{R_c}{R_p}\right)^3 \sqrt{2\mu_o c f_{\mathrm{ohm}} \rho_{\mathrm{core}}^{1/3}} \left[\frac{(q_{\mathrm{cmb}} - q_{\mathrm{ad}}) q_{\mathrm{ad}} R_c}{k_c T_c}\right]^{1/3}, \tag{9}$$

which can be reduced to $B_d = 1.21 \times 10^{-5} \left[q_{\mathrm{ad}} \left(q_{\mathrm{cmb}} - q_{\mathrm{ad}}\right)\right]^{1/3}$, where B_d is the expected dipolar magnetic field intensity (in tesla) assuming f_{dip} is one-seventh of the total magnetic field intensity.

Many workers have attempted to examine the possibility of an internally generated lunar magnetic field [*Konrad and Spohn*, 1997; *Williams et al.*, 2001; *Stegman et al.*, 2003; *Dwyer et al.*, 2011; *Le Bars et al.*, 2011; *Laneuville et al.*, 2013; *Zhang et al.*, 2013], finding that core convection generally cannot be sustained after 4 Ga. Additionally, varied assumptions in equation (8) lead to variations in the minimum heat flux (1–9 mW/m^2) required for sustaining a core dynamo. Herein, for a 350-km core, we use a critical threshold value of 2.4 mW/m^2 as a sufficient constraint to sustain a core dynamo. This is likely a lower bound for the critical core heat flux and is dependent on the assumed values for variables in equation (8). The actual value

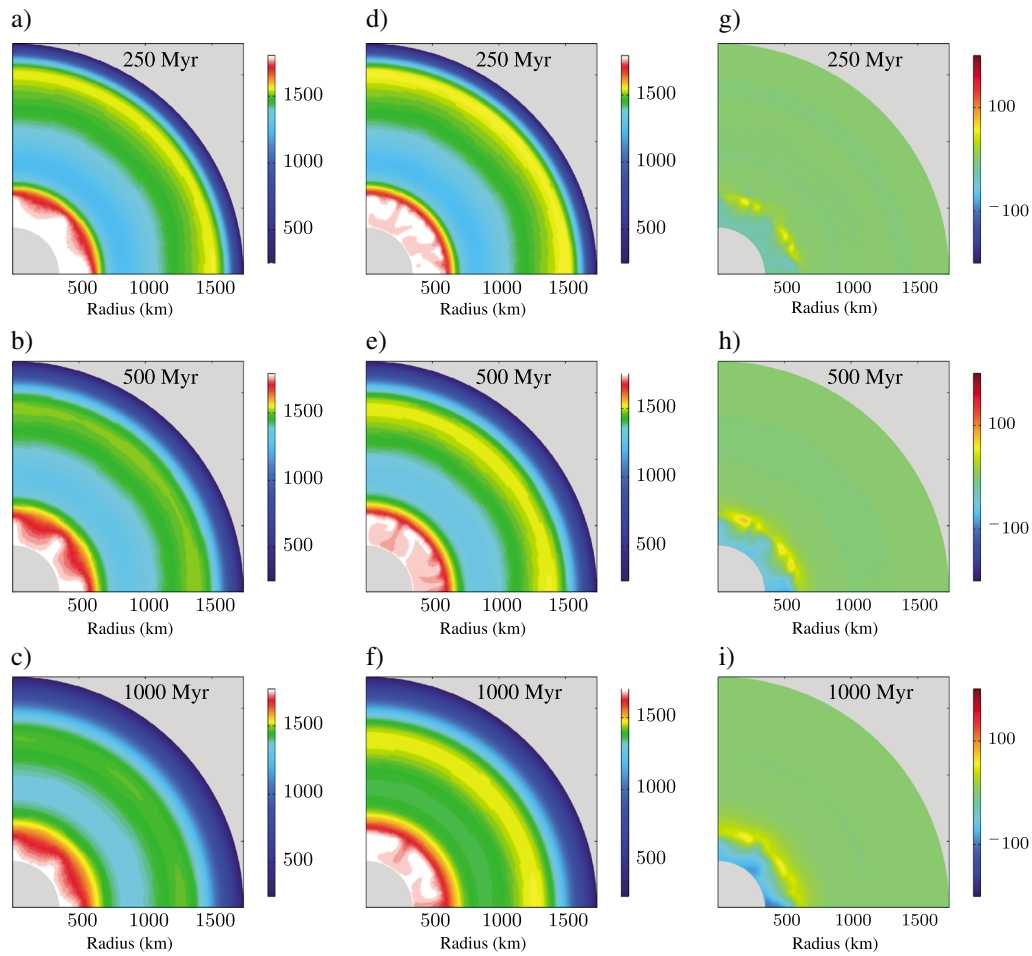

Figure 4. Reference case: Half-hemisphere temperature view of the lunar mantle model. ΔT_{cmb} = 0 K. Shown are lunar interior panels with pseudocolor temperature (K) at 0.25, 0.50, and 1.0 Gyr after model initialization. (a–c) Case D07 (no water enrichment). (d–f) Case D08 (200-km water-enriched layer with 40 ± 20 ppm water). (g–i) Temperature difference between cases D08 and D07, highlighting the increased convection vigor of the water-rich layer. The radial average of the temperature difference with time is shown in Figure 5b.

for the critical core heat flux has been suggested to be as high as 9 mW/m^2 [*Stegman et al.*, 2003]; nonetheless, the likely minimal value of 2.4 mW/m^2 allows us to examine all cases that could potentially sustain a convective core dynamo. We adjust this value accordingly for cases of a 450-km core to 3.0 mW/m^2.

3. Results

We investigate the effect of water on lower-mantle thermal evolution through end-member scenarios of initial density and temperature profiles within the Moon. Estimates of lunar magma ocean (LMO) depth based upon the thickness of the feldspar-rich flotation crust modeling by *Elkins-Tanton et al.* [2011] suggests a LMO depth of up to 1000 km, while more conservative estimates only yield up to 250 km [*Warren*, 1985]. A 1000-km-deep LMO crystallizes with an unstable density profile, leading to gravitationally driven overturn of the magma ocean cumulates and thereby permitting cooler, near-surface material to be transported deeper in the mantle. While a similar gravitationally driven overturn may occur for shallower LMOs, we model a 400-km-deep LMO as a chemically homogeneous mantle.

Accordingly, we choose the following two end-member scenarios for initialization of our evolution model (Figure 1) with a nominal reference viscosity range of 10^{19}–10^{21} Pa s and assume a model start time of 4.4 Ga, consistent with completion of magma ocean solidification and overturn [e.g., *Elkins-Tanton et al.*, 2011]:

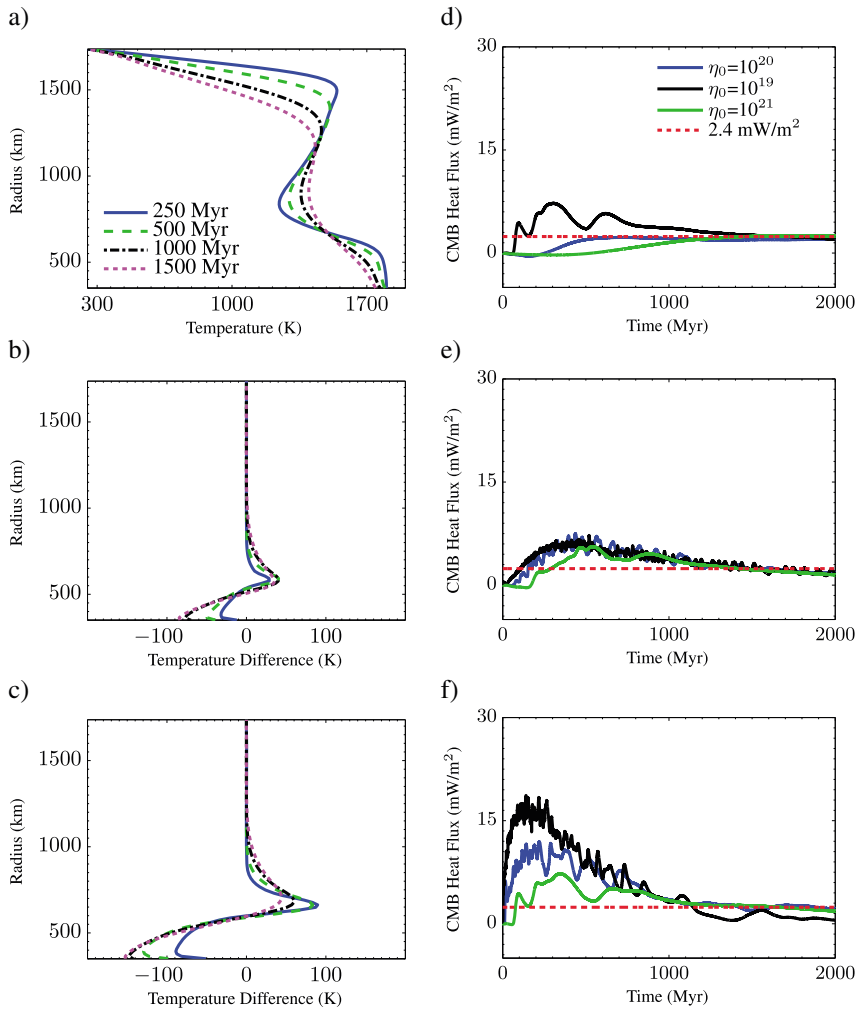

Figure 5. Temperatures and heat fluxes for deep lunar magma ocean model with ΔT_{cmb} = 0 K. (a and d) Case D07: No water enrichment. (b and e) Case D08: 200-km water-enriched layer with 40 ± 20 ppm water. (c and f) Case D09: 500-km water-enriched layer with 40 ± 20 ppm water. The radially averaged temperature in time is shown for Case D01 in Figure 5a with Figures 5b and Figure 5c tracking the temperature differences with time relative to Case D07. In Figure 5d–5f, CMB heat flux is shown in models with different reference viscosities $\eta_0 = 10^{19}$ (black line), $\eta_0 = 10^{20}$ (blue line), and $\eta_0 = 10^{21}$ (green line) as a function of model start time with the minimum heat flux needed to sustain a core dynamo (red dash-dotted line).

1. Shallow Magma Ocean. A chemically homogeneous mantle at a temperature of 1600 K below 400 km depth and with a temperature that varies linearly from 1450 K to 1600 K from the surface to 400-km depth.
2. Deep Magma Ocean. A compositionally stratified (chemically heterogeneous) mantle at a postmagma ocean overturn temperature and density (Figure 1). From just below the surface, the density increases linearly until 1000-km depth.

Using the fully nondimensionalized Arrhenius equation (5), we explore the effect of water enrichment for a range of CMB temperature boundary conditions. While the lunar core may be capable of initially retaining a 700-K higher temperature relative to the lower mantle [*Konrad and Spohn*, 1997], we examine moderate cases initiated with a temperature difference across the core-mantle boundary, ΔT_{cmb}, at 200 K and below. In section 3.2.2, we examine the effect of varying core radii on our results and employ a temperature-damped viscosity equation (7) as a proxy for a deep LMO scenario in which the magma ocean cumulates do not fully retain their temperature postoverturn.

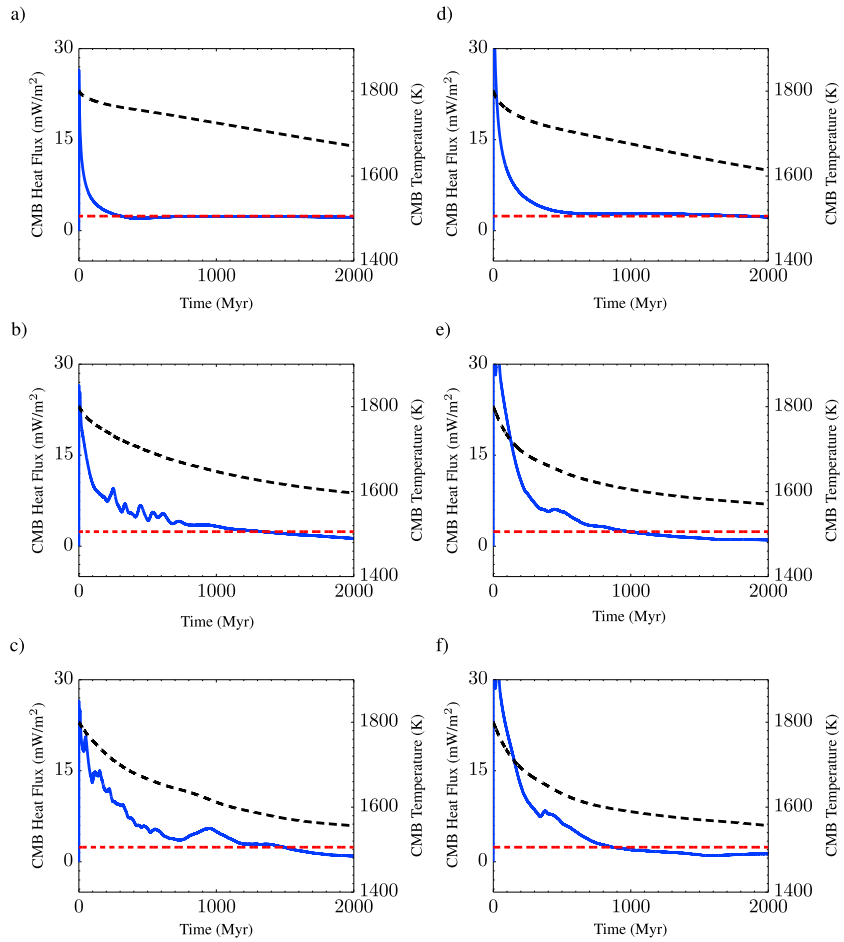

Figure 6. CMB heat fluxes for deep lunar magma ocean model and reference viscosity of 10^{20} Pa s. The CMB heat flux (blue solid line) is shown on the left axis with the minimum heat flux needed to sustain a core dynamo (red dash-dotted line) and the core temperature (black dashed line) on the right axis. (a–c) Models with $\Delta T_{\mathrm{cmb}} = 100$ K. (d–f) Models with $\Delta T_{\mathrm{cmb}} = 200$ K. Figure 6a shows Case D37: No water enrichment. Figure 6b shows Case D38: 200-km water-enriched layer with 40 ± 20 ppm water. Figure 6c shows Case D39: 500-km water-enriched layer with 40 ± 20 ppm water. Figure 6d shows Case D43: No water enrichment. Figure 6e shows Case D44: 200-km water-enriched layer with 40 ± 20 ppm water. Figure 6f shows Case D45: 500-km water-enriched layer with 40 ± 20 ppm water.

3.1. Shallow Lunar Magma Ocean

For a chemically homogeneous mantle with no initial temperature difference across the CMB, heat flow in the lunar mantle is dominated by conduction. As a result, the core heat flux is relatively weak and is below the minimum needed to sustain a dynamo for all of lunar history (Figure 2a).

In Figures 2d and 3d, we observe that a higher initial CMB temperature difference and lower reference viscosity enhances the CMB heat flux in the first few hundred million years and exceeds the minimum CMB heat flux within the first 0.01 Gyr. We find a sustained core heat flux above the minimum required for convection only persisting to 3.8 Ga, which is not sufficient to explain the remanent magnetization in samples formed as late as 3.56 Ga [*Shea et al.*, 2012; *Suavet et al.*, 2013]. As expected from equation (9), the increased initial CMB temperature difference results in a slightly greater intensity for the dipolar magnetic field at the surface: 0.4 μT at <0.1 Gyr and 0.5 μT at <0.1 Gyr, for 100-K and 200-K initial CMB temperature differences, respectively.

3.1.1. Shallow LMO: Water

When water is relatively enriched in a layer above the CMB, the lower viscosity promotes convection in the lower mantle, resulting in a higher CMB heat flux and a lower core temperature (Figures 2d–2f and Table 4). In this case, the upper mantle remains in a conductive heat transport regime, while the mantle below 600 km convects for up to 0.8 Gyr.

Table 4. Shallow Lunar Magma Ocean: CMB Heat Fluxes

Scenario	Input Parameters		Dynamo Regime			Maximum Surface Dipolar Field Intensity (μT)
	CMB ΔT (K)	Water Layer[a] (km)	A_H	Begin (Myr)	End (Myr)	
S01	0	0	1	-	-	-
S02	0	250	10^{-2}	90	170	0.2
S03	0	500	10^{-2}	80	180	0.2
S04	0	100	10^{-2}	100	220[b]	0.2
S05	0	500	10^{-1}	90	170	0.2
S06	0	100	10^{-1}	120	150	0.1
S25	100	0	1	0	190	0.4
S26	100	250	10^{-2}	0	410	0.4
S27	100	500	10^{-2}	0	340	0.4
S28	100	100	10^{-2}	0	480	0.4
S29	100	500	10^{-1}	0	410	0.4
S30	100	100	10^{-1}	0	490	0.4
S31	200	0	1^{-2}	0	470	0.5
S32	200	250	10^{-2}	0	440	0.5
S33	200	500	10^{-2}	0	500	0.5
S34	200	100	10^{-2}	0	380[c]	0.5
S35	200	500	10^{-1}	0	840	0.5
S36	200	100	10^{-1}	0	480	0.5

[a]Refers to layer height above CMB.
[b]Also active from 1.4 to 1.5 Gyr.
[c]Also active from 0.7 to 1.0 Gyr.

As shown in Figures 2a–2c, in the case of no initial temperature difference across the CMB, the addition of a water-enriched region above the core yields a CMB heat flux incapable of sustaining a core dynamo for much of lunar history, and generally, the addition of a water-enriched layer near the CMB has a minimal effect on extending the dynamo era. We find a similar result with ΔT_{cmb} = 200 K, with the exception of a 50% reduction in the amount of water (factor of 10 viscosity reduction) constrained to a 500-km layer, which allows for a core dynamo to be sustained through 3.56 Ga, the age of the youngest samples showing evidence for a lunar magnetic field. With an intermediate value of ΔT_{cmb} = 100 K, the duration of the dynamo period is more than doubled in the presence of water enrichment.

Thus, our results suggest that for an otherwise chemically homogeneous mantle, the role of water is strongly linked to the initial CMB temperature difference, as well as the water enrichment concentration and depth. We find that under certain conditions (i.e., ΔT_{cmb} = 200 K), a water-enriched layer may extend the core

Table 5. Deep Lunar Magma Ocean: CMB Heat Fluxes

Scenario	Input Parameters		Dynamo Regime			Maximum Surface Dipolar Field Intensity (μT)
	CMB ΔT (K)	Water Layer (km)	A_H	Begin (Myr)	End (Myr)	
D07	0	0	1	-	-	-
D08	0	250	10^{-2}	150	1640	0.3
D09	0	500	10^{-2}	10	1880	0.3
D10	0	100	10^{-2}	610	1090	0.1
D11	0	500	10^{-1}	80	1680	0.3
D12	0	100	10^{-1}	790	1160	0.1
D37	100	0	1	0	310	0.4
D38	100	250	10^{-2}	0	1340	0.5
D39	100	500	10^{-2}	0	1490	0.5
D40	100	100	10^{-2}	0	350	0.4
D41	100	500	10^{-1}	0	1220	0.4
D42	100	100	10^{-1}	0	1690	0.4
D43	200	0	1	0	1840	0.5
D44	200	250	10^{-2}	0	990	0.5
D45	200	500	10^{-2}	0	870	0.5
D46	200	100	10^{-2}	0	1690	0.5
D47	200	500	10^{-1}	0	800	0.5
D48	200	100	10^{-1}	0	1810	0.5

Table 6. Temperature-Damped Viscosity: CMB Heat Fluxes

Scenario	Input Parameters			Dynamo Regime			Maximum Surface Dipolar Field Intensity (μT)
	Core Radius (km)	CMB ΔT (K)	Water Layer (km)	A_H	Begin (Myr)	End (Myr)	
D13	350	0	0	1	140	1260	0.5
D14	350	0	250	10^{-2}	80	1150	0.5
D15	350	0	500	10^{-2}	0	840	0.6
D16	350	0	100	10^{-2}	90	670	0.6
D17	350	0	500	10^{-1}	20	970	0.5
D18	350	0	100	10^{-1}	110	940	0.6
D49	350	200	0	1	0	1040	0.5
D50	350	200	250	10^{-2}	0	690	0.6
D51	350	200	500	10^{-2}	0	680	0.7
D52	350	200	100	10^{-2}	0	800	0.6
D53	350	200	500	10^{-1}	0	930	0.6
D54	350	200	100	10^{-1}	0	730	0.6
D13-450	450	0	0	1	140	1270	1.2
D14-450	450	0	250	10^{-2}	0	1230	1.2
D15-450	450	0	500	10^{-2}	0	760	2.1
D16-450	450	0	100	10^{-2}	70	670	1.5
D17-450	450	0	500	10^{-1}	20	860	1.6
D18-450	450	0	100	10^{-1}	90	1210	1.2
D49-450	450	200	0	1	0	1200	1.3
D50-450	450	200	250	10^{-2}	0	1140	1.7
D51-450	450	200	500	10^{-2}	0	670	2.2
D52-450	450	200	100	10^{-2}	0	820	1.6
D53-450	450	200	500	10^{-1}	0	880	1.8
D54-450	450	200	100	10^{-1}	0	950	1.3

dynamo period by up to 0.5 Gyr. Although water enrichment may increase the duration of a core dynamo, the maximum dipolar, magnetic field intensity is not increased by more than 0.2 μT at the surface.

3.2. Deep Lunar Magma Ocean

With the postoverturn deep LMO and $\Delta T_{cmb} = 0$ K, the initial mantle state has a nonmonotonic, radial temperature profile (Figure 1) with cold layers of magma ocean cumulates, formerly near the surface, embedded in warmer areas of the lower mantle. Within the first few million years, the crust conductively removes the excess heat from the near-surface overturned material and approaches a steady state thermal profile, while the upper and middle mantle maintain a conductive heat transport regime with periodic and sluggish lower mantle convection that may persist for the first 0.8 Gyr (Figure 4). After approximately 1.8 Gyr, the cold layers are heated by a combination of conduction and sluggish convection.

For the case with no initial CMB temperature difference, the heating of the sequestered cold layer allows for a delayed core dynamo to begin within 0.1 Gyr for a reference viscosity of 10^{19} Pa s. As shown in Figure 5d, this case does not allow for a convective core dynamo with a reference viscosity higher than 10^{19} Pa s within the first 1 Gyr. While the region below the sequestered cold layer convects, the cold layer is inhibited from participating in convection due to its higher viscosity. Unlike the shallow LMO scenario, a larger thermal gradient at depth can be maintained due to the sequestered cold layer. This thermodynamical behavior enables a mantle without water enrichment to sustain a CMB heat flux within the core dynamo regime for approximately 1.8 Gyr (Figure 5d) for a reference viscosity of 10^{19} Pa s.

Given the more vigorous convection catalyzed by the higher ΔT_{cmb}, the final core temperature is decreased as ΔT_{cmb} increases. As shown in Figure 6d, for an initial CMB temperature difference of 200 K, the initiation of a core dynamo is accelerated by the earlier onset of lower mantle convection and can continue through 2.6 Ga (Table 5) by maintaining a CMB heat flux just above the minimum for over 1 Gyr. Similar to the shallow LMO, when $\Delta T_{cmb} = 200$ K, a core dynamo is capable of producing a maximum dipolar magnetic field intensity of 0.5 μT at the surface.

3.2.1. Deep LMO: Water

By incorporating water within the deep lunar interior through a reduction in viscosity, the lower mantle more readily sustains a separate convective layer from the remainder of the mantle (Figures 4g–4i). We analyze scenarios for approximately 20 and 40 ± 20 wt ppm (factor of 100 viscosity reduction), within layers of 100 km, 250 km, and 500 km above the CMB. To gauge the effect of water content in the deep

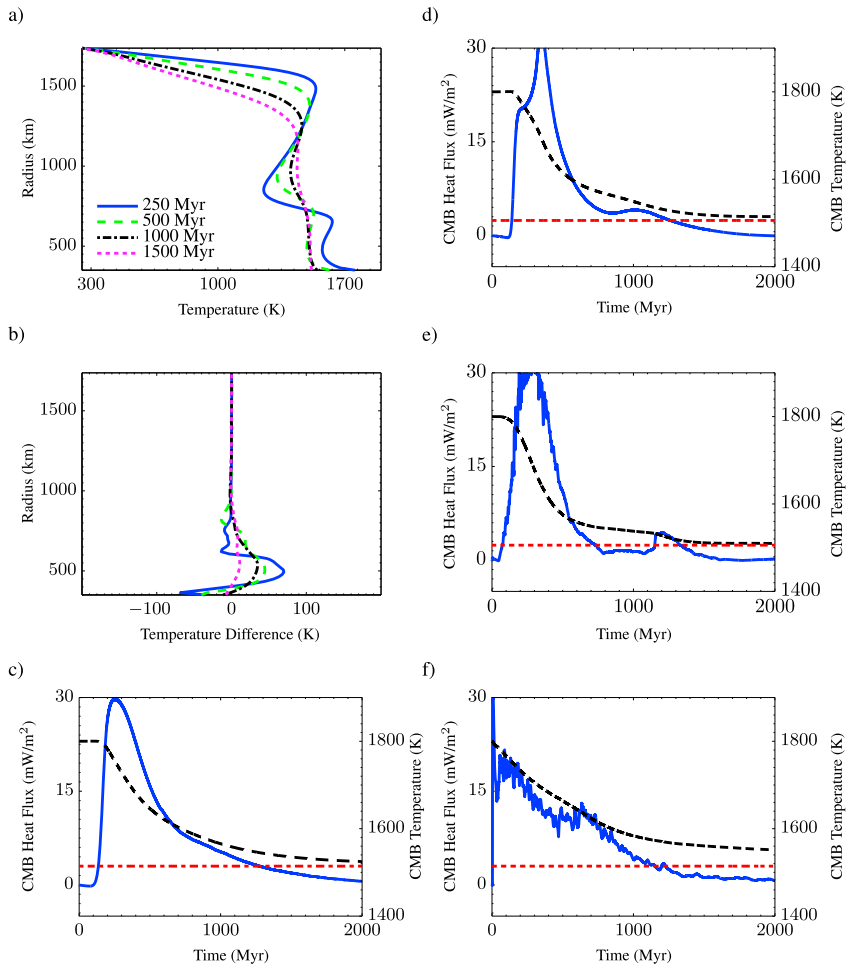

Figure 7. Temperatures and CMB heat fluxes for the temperature-damped, deep lunar magma ocean model with ΔT_{cmb} = 0 K and reference viscosity of 10^{20} Pa s. (a and d) Case D13: 350-km core radius and no water enrichment. (b and e) Case D14: 350-km core radius and 250-km water-enriched layer with 40 ± 20 ppm water. (c) Case D13-450: 450-km core radius and no water enrichment. (f) Case D14-450: 450-km core radius and 250-km water-enriched layer with 40 ± 20 ppm water. The temperature evolution in model time is shown with radius for Case D13 in Figure 7a with Figure 7b showing the temperature difference of Case D14 at the same time relative to Case D13. In Figures 7c–7f, the CMB heat flux (blue solid line) is shown on the left axis with the minimum heat flux needed to sustain a core dynamo (red dash-dotted line) and the core temperature (black dashed line) on the right axis.

interior, we examine model cases relative to the unenriched water mantle case, alongside varying CMB temperature boundary conditions.

For cases with no initial CMB temperature difference, the addition of a water-enriched layer allows for a CMB heat flux above the minimum to persist for 1.6 Gyr, and this layer is critical to the existence of a convective core dynamo for reference viscosities below 10^{21} Pa s. Although the reference viscosity range (10^{19}–10^{21} Pa s) we examine has a minimal impact on the duration of a convective core dynamo period (Figures 5e and 5f), the CMB heat flux is enhanced with progressively lower reference viscosities. Water enrichment has a negligible effect on the maximum magnetic field intensity for no initial CMB temperature difference but allows for relatively higher magnetic field intensities through the higher CMB heat flux in the first 1 Gyr.

With a 200-K initial CMB temperature difference, water enrichment generally increases the average CMB heat flux at the expense of shortening the core dynamo time span due to the more rapid heat loss from the core. This trend is not apparent with a 100-K ΔT_{cmb}, likely due to these cases remaining near a steady state and within a few percent of the minimum heat flux as shown in Figures 6a–6c. Generally, the result of a lower mantle with a relative enrichment in water is a region of reduced viscosity above the core that

convects heat away from the CMB into a convecting or conducting overlying mantle. A relative enrichment of water enables heat to be transported out of the core at an increased rate, catalyzed by the sequestered cold-mantle layer. For 40 ppm water in 250-km and 500-km layers above the core, the CMB heat flux generally allows a core dynamo to be initially active, lasting until 3.5–2.5 Ga, depending on the initial ΔT_{cmb} (Table 5).

3.2.2. Temperature-Damped Convection

We re-examine the deep LMO scenario for 350-km and 450-km core radii, this time using a temperature-damped viscosity (see equation (7)). For a postoverturn temperature profile, the upper and middle mantle remain in the conductive heat transport regime, with minimal lower mantle convection for the first 0.3 Gyr. As a consequence of the temperature dampening, the sequestered cold layer is able to participate in convection, leading to a major upwelling and CMB heat flux peak occurring at ~0.35 Gyr followed by a rapid decline in heat flux and thus magnetic field intensity.

When water is enriched in a layer above the CMB, heat is removed with a greater efficiency, resulting in a higher CMB heat flux and a lower core temperature. For 40 ppm water in 250-km and 500-km layers above the core, the CMB heat flux is capable of sustaining a core dynamo within the first 0.1 Gyr (Figure 7), but the relative water enrichment may reduce the lifetime of the core dynamo by 0.6 Gyr compared to the nonenrichment case. As shown in Table 6, in all but one case, increasing the initial temperature difference across the CMB reduces the end time of the core dynamo era by ~0.2 Gyr on average, while generally producing higher heat fluxes and hence stronger magnetic fields. Relative to the nominal deep LMO scenarios presented earlier, the temperature-damped cases allow for the mantle to transfer more heat earlier in lunar history, constraining the end time for a possible dynamo era to ~3.1 Ga. Contrary to the undamped case, for a deep LMO with a 350-km core radius, the addition of a water-enriched layer can increase the maximum dipolar intensity of the magnetic field by 0.1 μT for a 200-K initial CMB temperature difference.

For the case of a larger core radius of 450 km, the CMB heat flux for an unenriched water case is negligibly affected (Figure 7), while for the 250-km water-enriched layer case, the CMB heat flux peak locations and amplitudes vary. The greater variance in heat flux of the water-enriched case is due to the increase in total water content volume resulting from a larger core radius. The larger core radius shifts the top and bottom of the water-enriched layer to a larger radius, so for a constant layer thickness, there is a larger overall volume for the water-enriched layer. While the variation in heat flux is minimal, the 450-km core radius results in stronger surface magnetic fields by a factor of 2–3 relative to the 350-km core case. The increased magnetic field intensities are primarily a result of the increased core radius (see equation (9)) and demonstrate that for the structure assumed, the distance of the outer core to the surface is a critical factor in determining the maximum field strength observed at the surface. This result derives from the fact that the surface field intensity scales as the cube of the ratio of core radius to the lunar radius.

4. Discussion

The recent reanalyses of Apollo-era samples for magnetization have likely identified the existence of an internally generated magnetic field on the Moon between ~4.2 and 3.56 Ga [*Shea et al.*, 2012; *Garrick-Bethell et al.*, 2009; *Suavet et al.*, 2013]. The existence of such a field produced by a lunar core dynamo has been thought to be untenable for thermally convective core dynamos, with heat fluxes at the CMB generally unable to sustain a heat flux in excess of the adiabat beyond 4.0 Ga [*Stegman et al.*, 2003; *Konrad and Spohn*, 1997; *Laneuville et al.*, 2013].

Homogeneous models of the lunar mantle, as an approximation of a shallow LMO, predominantly transport heat by conduction after approximately 4.0 Ga. These models consistently result in large CMB heat fluxes within the first few hundred million years and near-zero fluxes for the remainder of lunar history, generally independent of most model parameters. The addition of water has two main effects: (1) it may change the duration of a dynamo for a homogeneous mantle by up to 0.4 Gyr allowing for a convective core dynamo to be active during the most recently recorded magnetic field sample age of 3.56 Ga and (2) in the lower mantle it provides a mechanism to enhance the amount of heat advected away from the core, strengthening the dynamo field intensity.

Our heterogeneous model of the lunar mantle is capable of producing a CMB heat flux above the core adiabat lasting for nearly 1.9 Gyr. The initial thermal profile assumes the postoverturn LMO cumulates retain fully the temperature associated with their preoverturn depth. Whether gravitationally driven overturn of

the LMO can occur while retaining the preoverturn temperature of the cumulates depends on the layer thickness, start time, and duration of overturn. Our analysis of the case in which the preoverturn LMO temperature is retained shows that within 1 billion years, a cold layer embedded in the deep interior is heated by a combination of conduction and convection, which helps to stimulate convection in the lower mantle. The heating of the deep cold layer allows for a delayed core dynamo to begin within 0.1 Gyr after magma ocean solidification and overturn. Without water enrichment, this scenario also allows for the possibility that a core dynamo existed for 1.8 Gyr, which may still be consistent with Apollo-era paleomagnetic data given that such a weak field would likely be below the detectable threshold [*Tikoo et al.*, 2012]. If the temperature dependence of viscosity is damped (section 3.2.2) to simulate scenarios in which the thermal gradient of the postoverturn LMO mantle is partially attenuated compared to our nominal post-LMO cases (section 3.2), our convective dynamo persists until 3.1 Ga.

In examining the role of water on the thermal evolution of the interior, we find that water enrichment at depth is likely to further decrease the temperature of the lower mantle over time and, depending on the water concentration and regional extent, shorten or lengthen the duration of a possible core dynamo. With a range of density and temperature profiles, the addition of water in the deep interior facilitates the transport of heat out of the deep mantle and provides a stronger CMB heat flux. Using equation (9), an upper limit for the magnetic field intensity can be produced from our core heat flux. For a deep LMO case with 40 ppm water in a 500-km layer above a 350-km core, the heat flux could promote a 0.7-μT dipolar magnetic field at the surface, compared with up to 0.5 μT in cases without water enrichment. Furthermore, we find varying the core radius (see equation (9)) results in a minimal change to the core heat flux but yields a significant increase in the surface magnetic field strength resulting in dipolar fields in excess of 1 μT. However, consistent with prior convective core dynamo models, our resultant dipolar fields are not sufficient to explain the inferred lunar paleofields (>10 μT) [*Garrick-Bethell et al.*, 2009; *Shea et al.*, 2012; *Suavet et al.*, 2013].

The very low Ti glasses recently discovered to contain water are theorized to originate from a heterogeneous mantle source, including a KREEP component, at less than 520-km depth [*Saal et al.*, 2008; *Shearer*, 2006; *Shearer and Papike*, 1993; *Elkins et al.*, 2000]. If only a small amount of KREEP was retained near the surface, the remainder along with its radioactive element and water content may have foundered with a dense layer of cumulates [*Stegman et al.*, 2003; *Zhang et al.*, 2013]. Given our results, it is likely that under these circumstances, water could have played an influential role in promoting a higher CMB heat flux and could have promoted core dynamo activity well beyond 3.7 Ga.

With the exception of a KREEP layer at the near surface, our temperatures do not exceed the bulk solidus, and thus, melt quantities are neglected. For larger quantities of melt, the partitioning of water and the amount of melt will play dominant roles in determining whether a viscosity reduction or increase is likely for melt under hydrous conditions [*Hirth and Kohlstedt*, 1996]. While our models do not directly predict near-surface magmatism in early lunar history, as geological evidence indicates occurred on the Moon [*Head*, 1975; *Wilhelms and McCaulay*, 1987; *Jolliff et al.*, 2000], our models may be compatible with near-surface magmatism induced by an ilmenite-bearing cumulate layer [*Zhang et al.*, 2013]. Additionally, the possible decoupling of interior and near-surface cooling of the early Moon suggest these are not irreconcilable differences.

While we choose a core adiabatic heat flux similar to *Dwyer et al.* [2011], our value is lower than the convective core dynamo models of *Stegman et al.* [2003] and *Laneuville et al.* [2013]. The variability in the core adiabatic heat flux in convective dynamo models is a result of differences in assumed core properties including radius, density, specific heat, thermal expansion, and thermal conductivity. The largest uncertainty is due to core thermal conductivity, which has generally been assumed to be between 25 and 50 W/m K based on assumed Earth values [*Anderson*, 1998; *Stacey and Anderson*, 2001]. Recent results from *de Koker and Steinle-Neumann* [2012] suggest the core conductivity values for Earth have likely been underestimated, though coincidentally, we note this range may be appropriate for lunar core conditions based on their computational results (50 W/m K) and experimental data (30–35 W/m K) included therein. The core thermal conductivity has been used to justify the larger core adiabatic heat flux of *Zhang et al.* [2013], while most authors have opted to use a median or a range of values [*Laneuville et al.*, 2013; *Stegman et al.*, 2003; *Dwyer et al.*, 2011]. As the core cools and the inner solid core grows, the growing solid inner core will reduce the minimum CMB heat flux necessary to maintain a superadiabatic liquid outer core [*Weber et al.*, 2011; *Dwyer*

et al., 2011]. Although the critical core heat flux will be a function of inner core solidification, this effect is generally not accounted for in dynamo models, likely resulting in the overestimation of the critical heat flux with time. Additionally, this effect could potentially allow a chemically homogeneous mantle to sustain a core dynamo more readily. By employing a minimum of 25 W/m K for the core thermal conductivity, we examine all cases that could potentially sustain a convective core dynamo. While we note that a higher core thermal conductivity or changes in other assumed values may result in a higher core adiabatic heat flux, our thermal evolution models are independent of the core thermal conductivity. Our overall conclusions remain unchanged for values of the core adiabatic heat flux through 5 mW m^{-2} resulting from changes in the core thermal conductivity (Figures 2, 3, and 5–7).

Furthermore, compared to convective dynamo models of *Stegman et al.* [2003] and *Laneuville et al.* [2013], our models generally maintain a higher CMB heat flux due to the inclusion of water and a compositionally stratified mantle. While the comprehensive study of *Zhang et al.* [2013] investigates the foundering of a near-surface ilmenite-bearing cumulate layer to the CMB and results in higher CMB heat fluxes than our model, their model is aided by higher lower mantle temperatures, exceeding our CMB temperature by 500 K.

5. Summary

From our results, we find that the addition of water within the lunar mantle can result in a CMB heat flux that is able to sustain a core dynamo beyond 3.56 Ga. Enriched water in the lower mantle acts as a catalyst for transporting heat out of the deep mantle due to the reduced viscosity from protonic weakening [*Kohlstedt*, 2006]. The cases that we examine demonstrate that with the consideration of a chemically layered mantle or water-enriched lower mantle, the core heat flux is no longer a limiting factor in sustaining a convective core dynamo beyond the period currently indicated by the Apollo samples.

A homogeneous, dry model of the lunar mantle is predominantly conductive after approximately 4.0 Ga, after which it is generally unable to support a convective core dynamo without external mediation of a thermal blanket [*Stegman et al.*, 2003; *Zhang et al.*, 2013], impact-induced rotation changes [*Le Bars et al.*, 2011], or, as we show in this study, the addition of mantle water or a postoverturn lunar magma ocean. The homogeneous mantle models tend to result in large CMB heat fluxes within the first few hundred million years, and very low fluxes for the rest of lunar history, consistent with prior models [*Konrad and Spohn*, 1997; *Stegman et al.*, 2003; *Laneuville et al.*, 2013].

We find that a deep lunar magma ocean after gravitationally driven overturn may sustain a core dynamo on timescales longer than the latest paleomagnetic data [*Shea et al.*, 2012; *Suavet et al.*, 2013], through 2.5 Ga. Based on the core dynamo scaling model of *Christensen et al.* [2009] and assuming a 350-km core radius, our results yield a maximum dipolar surface magnetic field intensity of 0.7 μT. Additionally, we find that the observed maximum magnetic field strength at the surface is strongly dependent on the lunar core radius, and with a 450-km core, the dipolar intensity may be up to ~2 μT.

If water was transported or retained preferentially in the Moon's deep interior, even in small amounts (20 ppm), it would have played a significant role in transporting heat out of the deep interior and reducing the lower mantle temperature. Water enriched in the lower mantle could have influenced the timing by over 1.0 Gyr and enhanced the surface magnetic field intensity of a convective core dynamo.

Acknowledgments
We thank L. Elkins-Tanton for temperature and density data provided for a postoverturn lunar magma ocean and S. Zhong for assistance in the Citcom2D thermochemical evolution model. We also thank J.C. Andrews-Hanna, T.L. Grove, and J.T. Perron for their assistance and comments. This work was supported by the NASA Lunar Science Institute and a NASA Lunar Advanced Science and Exploration Research grant to BPW.

References

Anderson, O. L. (1998), The Grüneisen parameter for iron at outer core conditions and the resulting conductive heat and power in the core, *Phys. Earth Planet. Inter.*, *109*(3–4), 179–197.

Bercovici, D., and S.-I. Karato (2003), Whole-mantle convection and the transition-zone water filter, *Nature*, *425*(6953), 39–44.

Borch, R. S., and H. W. Green II (1989), Deformation of peridotite at high pressure in a new molten salt cell: Comparison of traditional and homologous temperature treatments, *Phys. Earth Planet. Inter.*, *55*(3-4), 269–276.

Cameron, A. (1986), The impact theory for origin of the Moon, in *Origin of the Moon*, edited by W. K. Hartmann, R. J. Phillips, and G. J. Taylor, 609 pp., The Lunar and Planetary Institute, Kona, HI.

Cameron, A. G. W., and W. R. Ward (1976), Origin of the Moon, *Abst. Lunar Planet. Sci. Conf.*, *7*, 120–122.

Canup, R. M. (2004), Dynamics of lunar formation, *Annu. Rev. Astron. Astrophys.*, *42*(1), 441–475.

Canup, R. M., and E. Asphaug (2001), Origin of the Moon in a giant impact near the end of the Earth's formation, *Nature*, *412*(6848), 708–712.

Christensen, U. R., V. Holzwarth, and A. Reiners (2009), Energy flux determines magnetic field strength of planets and stars, *Nature*, *457*(7226), 167–169.

Cournède, C., J. Gattacceca, and P. Rochette (2012), Magnetic study of large Apollo samples: Possible evidence for an ancient centered dipolar field on the Moon, *Earth Planet. Sci. Lett.*, *331*, 31–42.

de Koker, N., and G. Steinle-Neumann (2012), Electrical resistivity and thermal conductivity of liquid Fe alloys at high P and T, and heat flux in Earth's core, *Proc. Natl. Acad. Sci. U.S.A.*, *109*, 4070–4073.

Dwyer, C. A., D. J. Stevenson, and F. Nimmo (2011), A long-lived lunar dynamo driven by continuous mechanical stirring, *Nature*, *479*(7372), 212–214.

Elkins, L. T., V. A. Fernandes, J. W. Delano, and T. L. Grove (2000), Origin of lunar ultramafic green glasses: Constraints from phase equilibrium studies, *Geochim. Cosmochim. Acta*, *64*(13), 2339–2350.

Elkins-Tanton, L., E. M. Parmentier, and P. Hess (2003), Magma ocean fractional crystallization and cumulate overturn in terrestrial planets: Implications for Mars, *Meteorit. Planet. Sci.*, *38*(12), 1753–1771.

Elkins-Tanton, L., and T. L. Grove (2011), Water (hydrogen) in the lunar mantle: Results from petrology and magma ocean modeling, *Earth Planet. Sci. Lett.*, *307*, 173–170.

Elkins-Tanton, L. T., S. Burgess, and Q.-Z. Yin (2011), The lunar magma ocean: Reconciling the solidification process with lunar petrology and geochronology, *Earth Planet. Sci. Lett.*, *304*, 326–336.

Fei, H., M. Wiedenbeck, D. Yamazaki, and T. Katsura (2013), Small effect of water on upper-mantle rheology based on silicon self-diffusion coefficients, *Nature*, *498*(7453), 213–215.

Garrick-Bethell, I., B. P. Weiss, D. L. Shuster, and J. Buz (2009), Early lunar magnetism, *Science*, *323*(5912), 356–359.

Girard, J., J. Chen, P. Raterron, and C. W. Holyoke (2013), Hydrolytic weakening of olivine at mantle pressure: Evidence of [100](010) slip system softening from single-crystal deformation experiments, *Phys. Earth Planet. Inter.*, *216*, 12–20.

Greenwood, J. P., S. Itoh, N. Sakamoto, P. Warren, L. Taylor, and H. Yurimoto (2011), Hydrogen isotope ratios in lunar rocks indicate delivery of cometary water to the Moon, *Nat. Geosci.*, *4*(2), 79–82.

Hauri, E. H., T. Weinreich, A. E. Saal, M. C. Rutherford, and J. A. Van Orman (2011), High pre-eruptive water contents preserved in lunar melt inclusions, *Science*, *333*(6039), 213–215.

Head, J. W. (1975), Lunar mare deposits: Areas, volumes, sequence, and implication for melting in source areas, paper presented at Conference on Origins of Mare Basalts and their Implications for Lunar Evolution, LPI Contributions number 234, Houston, Tex.

Hess, P. C., and E. M. Parmentier (2001), Thermal evolution of a thicker KREEP liquid layer, *J. Geophys. Res.*, *106*(E11), 28,023–28,032.

Hirth, G., and D. L. Kohlstedt (1995), Experimental constraints on the dynamics of the partially molten upper mantle: 2. Deformation in the dislocation creep regime, *J. Geophys. Res.*, *100*(B8), 15,441–15,449.

Hirth, G., and D. L. Kohlstedt (1996), Water in the oceanic upper mantle: Implications for rheology, melt extraction and the evolution of the lithosphere, *Earth Planet. Sci. Lett.*, *144*(1-2), 93–108.

Hood, L. L., and M. T. Zuber (2000), Recent refinements in geophysical constraints on lunar origin and evolution, in *Origin of the Earth and Moon*, edited by R. M. Canup and K. Righter, pp. 397–409, Univ. of Arizona Press, Tucson.

Jolliff, B. L., C. Floss, I. S. McCallum, and J. M. Schwartz (1999), Geochemistry petrology and cooling history of 141617373 a plutonic lunar sample with textural evidence of granitic-fraction separation by silicate-liquid immiscibility, *Am. Min.*, *84*, 821–837.

Jolliff, B. L., J. J. Gillis, L. A. Haskin, R. L. Korotev, and M. A. Wieczorek (2000), Major lunar crustal terranes: Surface expressions and crust-mantle origins, *J. Geophys. Res.*, *105*(E2), 4197–4216.

Karato, S.-I. (2010), Rheology of the deep upper mantle and its implications for the preservation of the continental roots: A review, *Tectonophysics*, *481*(1–4), 82–98, doi:10.1016/j.tecto.2009.04.011.

Karato, S.-I. (2013), Does partial melting explain geophysical anomalies?, *Phys. Earth Planet. Inter.*, doi:10.1016/j.pepi.2013.08.006, in press.

Khan, A., A. Pommier, and J. A. D. Connolly (2013), On the presence of a titanium-rich melt layer in the deep lunar interior, paper presented at 44th Lunar and Planetary Science Conference, LPI Contribution No. 1719, Woodlands, Tex.

Kohlstedt, D. L. (2006), The role of water in high-temperature rock deformation, *Rev. Mineral. Geochem.*, *62*, 377–396.

Konrad, W., and T. Spohn (1997), Thermal history of the Moon: Implications for an early core dynamo and post-accertional magmatism, *Adv. Space Res.*, *19*(10), 1511–1521.

Korenaga, J. (2009), Scaling of stagnant lid convection with Arrhenius rheology and the effects of mantle melting, *Geophys. J. Int.*, *179*, 154–170.

Korotev, R. L. (2000), The great lunar hot spot and the composition and origin of the Apollo mafic ("LKFM") impact-melt breccias, *J. Geophys. Res.*, *105*(E2), 4317–4345, doi:10.1029/1999JE001063.

Laneuville, M., M. A. Wieczorek, D. Breuer, and N. Tosi (2013), Asymmetric thermal evolution of the Moon, *J. Geophys. Res. Planets*, *118*, 1435–1452, doi:10.1002/jgre.20103.

Le Bars, M., M. A. Wieczorek, Ö. Karatekin, D. Cebron, and M. Laneuville (2011), An impact-driven dynamo for the early Moon, *Nature*, *479*, 215–218.

Longhi, J., and L. D. Ashwal (1985), Two-stage models for lunar and terrestrial anorthosites: Petrogenesis without a magma ocean, *J. Geophys. Res.*, *90*(S02), C571–C584, doi:10.1029/JB090iS02p0C571.

Lucey, P., et al. (2006), Understanding the lunar surface and space-Moon interactions, *Rev. Mineral. Geochem.*, *60*, 83–219.

Mackwell, S. J., D. L. Kohlstedt, and M. S. Paterson (1985), The role of water in the deformation of olivine single crystals, *J. Geophys. Res.*, *90*(B13), 11,319–11,333, doi:10.1029/JB090iB13p11319.

McCallum, I. S., and J. M. Schwartz (2001), Lunar Mg suite: Thermobarometry and petrogenesis of parental magmas, *J. Geophys. Res.*, *106*(E11), 27,969–27,983, doi:10.1029/2000JE001397.

Moresi, L., and V. Solomatov (1995), Numerical investigation of 2D convection with extremely large viscosity variations, *Phys. Fluids*, *7*(9), 2154–2162.

Neumann, G., M. Zuber, D. Smith, and F. Lemoine (1996), The lunar crust: Global structure and signature of major basins, *J. Geophys. Res.*, *101*(E7), 16,841–16,863, doi:10.1029/96JE01246.

Pahlevan, K., and D. Stevenson (2011), Chemical fractionation in the silicate vapor atmosphere of the Earth, *Earth Planet. Sci. Lett.*, *301*, 433–443.

Roberts, J. H., and S. Zhong (2004), Plume-induced topography and geoid anomalies and their implications for the Tharsis rise on Mars, *J. Geophys. Res.*, *109*, E03009, doi:10.1029/2003JE002226.

Roberts, J. H., and S. Zhong (2006), Degree-1 convection in the Martian mantle and the origin of the hemispheric dichotomy, *J. Geophys. Res.*, *111*, E06013, doi:10.1029/2005JE002668.

Runcorn, S. K. (1996), The formation of the lunar core, *Geochim. Cosmochim. Acta*, *60*(7), 1205–1208.

Saal, A. E., E. H. Hauri, M. L. Cascio, J. A. Van Orman, M. C. Rutherford, and R. F. Cooper (2008), Volatile content of lunar volcanic glasses and the presence of water in the Moon's interior, *Nature*, *454*(7201), 192–195.

Saal, A. E., E. H. Hauri, J. A. Van Orman, and M. J. Rutherford (2012), D/H ratios of the lunar volcanic glasses, paper presented at 43rd Lunar and Planetary Science Conference, LPI Contribution No. 1659, Woodlands, Tex.

Shea, E. K., B. P. Weiss, W. S. Cassata, D. L. Shuster, S. M. Tikoo, J. Gattacceca, T. L. Grove, and M. D. Fuller (2012), A long-lived lunar core dynamo, *Science*, *335*(6067), 453–456.

Shearer, C. K. (2006), Thermal and magmatic evolution of the Moon, *Rev. Mineral. Geochem.*, *60*(1), 365–518.

Shearer, C. K., and J. J. Papike (1993), Basaltic magmatism on the Moon: A perspective from volcanic picritic glass beads, *Geochim. Cosmochim. Acta*, *57*, 4785–4812.

Stacey, F. D., and O. L. Anderson (2001), Electrical and thermal conductivities of Fe–Ni–Si alloy under core conditions, *Phys. Earth Planet. Inter.*, *124*(3-4), 153–162.

Stegman, D. R., A. Jellinek, S. Zatman, J. R. Baumgardner, and M. A. Richards (2003), An early lunar core dynamo driven by thermochemical mantle convection, *Nature*, *421*, 143–146.

Suavet, C., B. P. Weiss, W. S. Cassata, D. L. Shuster, J. Gattacceca, L. Chan, I. Garrick-Bethell, J. W. Head, T. L. Grove, and M. D. Fuller (2013), Persistence and origin of the lunar core dynamo, *Proc. Natl. Acad. Sci. U.S.A.*, *110*(21), 8453–8458.

Taylor, S. R., G. J. Taylor, and L. A. Taylor (2006), The Moon: A Taylor perspective, *Geochim. Cosmochim. Acta*, *70*(24), 5904–5918.

Taylor, G. J., et al. (2013), Revised thickness of the lunar crust from GRAIL data: Implications for lunar bulk composition, paper presented at 44th Lunar and Planetary Science Conference, Houston, Tex.

Tikoo, S. M., B. P. Weiss, J. Buz, E. A. Lima, E. K. Shea, G. Melo, and T. L. Grove (2012), Magnetic fidelity of lunar samples and implications for an ancient core dynamo, *Earth Planet. Sci. Lett.*, *337*, 93–103.

Warren, P. (1985), The magma ocean concept and lunar evolution, *Annu. Rev. Earth Planet. Sci.*, *13*, 201–240.

Warren, P. H., and J. T. Wasson (1979), The origin of KREEP, *Rev. Geophys.*, *17*(1), 73–88, doi:10.1029/RG017i001p00073.

Weber, R. C., P.-Y. Lin, E. J. Garnero, Q. Williams, and P. Lognonne (2011), Seismic detection of the lunar core, *Science*, *331*(6015), 309–312.

Wieczorek, M. A., and R. J. Phillips (1998), Potential anomalies on a sphere: Applications to the thickness of the lunar crust, *J. Geophys. Res.*, *103*(E1), 1715–1724.

Wieczorek, M. A., and R. J. Phillips (2000), The "Procellarum KREEP Terrane": Implications for mare volcanism and lunar evolution, *J. Geophys. Res.*, *105*, 20,417–20,430.

Wieczorek, M. A., et al. (2013), The crust of the Moon as seen by GRAIL, *Science*, *339*(6120), 671–675.

Wilhelms, D. E., and J. F. McCaulay (1987), The Geology of the Moon, *U.S. Geol. Surv. Prof. Pap. 1348*, 302 pp.

Williams, J. G., D. H. Boggs, C. F. Yoder, J. T. Ratcliff, and J. O. Dickey (2001), Lunar rotational dissipation in solid body and molten core, *J. Geophys. Res.*, *106*(E11), 27,933–27,968.

Wood, J. A. (1972), Thermal history and early magmatism in the Moon, *Icarus*, *16*(2), 229–240.

Wood, J. A., J. S. Dickey, U. B. Marvin, and B. N. Powell (1970), Lunar anorthosites, *Science*, *167*(3918), 602–604.

Yang, W.-S., and J. R. Baumgardner (2000), A matrix-dependent transfer multigrid method for strongly variable viscosity infinite Prandtl number thermal convection, *Geophys. Astrophys. Fluid Dyn.*, *92*(3), 151–195.

Zhang, N., E. M. Parmentier, and Y. Liang (2013), A 3-D numerical study of the thermal evolution of the Moon after cumulate mantle overturn: The importance of rheology and core solidification, *J. Geophys. Res. Planets*, *118*, 1789–1804, doi:10.1002/jgre.20121.

Zhong, S., M. T. Zuber, L. Moresi, and M. Gurnis (2000a), Role of temperature-dependent viscosity and surface plates in spherical shell models of mantle convection, *J. Geophys. Res.*, *105*(B5), 11,063–11,082.

Zhong, S., E. M. Parmentier, and M. T. Zuber (2000b), A dynamic origin for the global asymmetry of lunar mare basalts, *Earth Planet. Sci. Lett.*, *177*, 131–140.

Zhong, S., D. A. Yuen, and L.-N. Moresi (2007), Numerical methods for mantle convection, *Treatise Geophys.*, *7*, 227–252.

Zuber, M. T., et al. (2013), Gravity field of the Moon from the Gravity Recovery and Interior Laboratory (GRAIL) mission, *Science*, *339*(6120), 668–671.